Author Manuscript

Author Manuscript

Author Manuscript

Author Manuscript

HHS Public Access

Author manuscript

Acta Biomater. Author manuscript; available in PMC 2020 January 15.

Published in final edited form as:

Acta Biomater. 2019 January 15; 84: 414–423. doi:10.1016/j.actbio.2018.11.041.

Compositionally Graded Doped Hydroxyapatite Coating using Laser and Plasma Spray Deposition

Dongxu Ke, **Ashley A. Vu**, **Amit Bandyopadhyay**, and **Susmita Bose***

W. M. Keck Biomedical Materials Research Laboratory, School of Mechanical and Materials Engineering, Washington State University, Pullman, WA 99164-2920, USA

Abstract

Plasma sprayed hydroxyapatite (HA) coating is known to improve the osteoconductivity of metallic implants. However, the adhesive bond strength of the coating is affected due to a mismatch in coefficients of thermal expansion (CTE) between the metal and the HA ceramic. In this study, a gradient HA coating was prepared on Ti6Al4V by laser engineered net shaping (LENS™) followed by plasma spray deposition. In addition, 1 wt.% MgO and 2 wt.% Ag_2O were mixed with HA to improve the biological and antibacterial properties of the coated implant. Results showed that the presence of an interfacial layer by LENS™ enhanced adhesive bond strength from 26 ± 2 MPa for just plasma spray coating to 39 ± 4 MPa for LENS™ and plasma spray coatings. Presence of MgO and Ag_2O did not influence the adhesive bond strength. Also, Ag^+ ions release dropped by 70% less with a gradient HA LENS™ layer due to enhanced crystallization of the HA layer. *In vitro* human osteoblast cell culture revealed presence of Ag_2O had no deleterious effect on proliferation and differentiation when compared to pure HA as control and provided antibacterial properties against *E. coli* and *S. aureus* bacterial strands. This study presents an innovative way to improve interfacial mechanical properties of plasma sprayed HA coating for load-bearing orthopedic implants.

Graphical Abstract

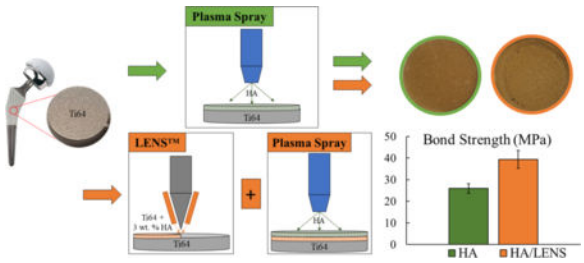

*Corresponding Author sbose@wsu.edu.

Publisher's Disclaimer: This is a PDF file of an unedited manuscript that has been accepted for publication. As a service to our customers we are providing this early version of the manuscript. The manuscript will undergo copyediting, typesetting, and review of the resulting proof before it is published in its final citable form. Please note that during the production process errors may be discovered which could affect the content, and all legal disclaimers that apply to the journal pertain.

Author Manuscript Author Manuscript Author Manuscript Author Manuscript

Keywords

Laser engineered net shaping; plasma sprayed coating; hydroxyapatite; adhesive bond strength; bone cell-materials interactions

1. Introduction

One of the most prominent human health concerns facing the population today surrounds musculoskeletal disorders. In the US alone, 310,800 total hip replacements were performed in 2010 with patients aged 45 and up [1]. Younger patients under 40 receiving hip implants is anticipated to increase which also means shorter implant life is expected due to the higher activity lifestyle [2]. Many factors can limit the life of load-bearing implants including stress shielding, poor osseointegration, or implant loosening.

To address these challenges, this study utilizes a novel gradient surface modification system whereby the gradient is produced by Laser Engineered Net Shaping (LENS™) and hydroxyapatite (HA) is used as a coating material. Gradient is used in this study to describe the embedding of HA between a Ti6Al4V substrate and plasma HA coating, reminiscent of a gradient going from 0 % HA to 3 wt. % HA to 100 % HA. LENS™ is a type of direct laser deposition additive manufacturing technique that has grown in a number of commercial, aerospace, and Department of Defense applications [3–6]. It utilizes a high power laser to melt powders for deposition of molten material and as the laser moves, the deposited material instantly solidifies creating a cross-sectional layer [7,8]. LENS™ not only provides the ability to manufacture complex 3D objects but can also be used to modify surfaces [9,10]. In addition, the composition of each layer can be varied easily, and the depth of the gradient layer can be changed, which makes it an excellent tool to manufacture metal-ceramic composite coatings. To the best of our knowledge, additive manufacturing with titanium and hydroxyapatite employing selective laser melting has been reported by only a few studies however LENS™ utilization has not been explored extensively [11,12]. We propose a system whereby Ti6Al4V substrate, a widely used titanium alloy for biomedical applications [13,14], is modified with a 3 wt.% HA doped Ti6Al4V LENS™ layer prior to plasma thermal spraying of a MgO/Ag_2O doped HA coating. This study expands and optimizes a previous study where a gradient HA coating was also prepared by LENS™ processing and plasma spray deposition however HA was not doped and had decomposed to tricalcium phosphate and calcium titanate after LENS™ processing [15].

HA has been widely used as a coating material in load-bearing implants to improve osteoconductivity which enhances osseointegration [16–18]. HA has excellent biocompatibility due to its compositional similarity to bone mineral. Additionally, HA has higher stability and lower dissolution rate compared to other calcium phosphate materials. Plasma sprayed coating has advantages of low cost, high deposition rate, and bulk production, enabling its use in industry for commercial orthopedic implants [19–22]. High adhesive bond strength is crucial to minimize spalling and increase the lifespan of the coating. A gradient HA layer will reduce thermally induced stresses between HA and

Author Manuscript Author Manuscript Author Manuscript Author Manuscript

Ti6Al4V thereby increasing the adhesive bond strength through decreasing crack formation at the coating / implant interface.

Doping the HA coating can improve osteoconductivity as well as provide other benefits such as reducing bacterial infection. Silver (Ag) is effective against a wide range of bacteria and has been approved for the use in various medical devices for 20 years. Compared to other antimicrobial agents, such as antibiotics, Ag contained HA coatings have long-term infection protection and will not decompose during implant sterilization techniques. Magnesium (Mg) is another dopant reported to improve osteoblast attachment, enhance ALP production, and induce nitric oxide production in endothelial cells comparable to the mechanism VEGF uses to induce angiogenesis [23].

The objective of this study is to understand the effects of a gradient HA coating utilizing LENS™ on Ti6Al4V load-bearing implants for improved mechanical properties. The hypothesis is the gradient layer will increase the adhesive bond strength of the plasma coating by providing a thermal barrier, reducing fast quenching, and increase crystallinity. Coating mechanical properties were evaluated as well as *in vitro* characterizations of antibacterial properties against *Escherichia coli (E. coli)* and *Staphylococcus aureus (S. aureus*), as well as biological properties utilizing a preosteoblast cell line. This novel gradient surface modification system can improve osseointegration for patients with active lifestyles and decrease the risk of implant failure from loosening or infection.

2. Materials and Methods

2.1 LENS™ Processed Gradient HA Layer

Ti6Al4V plates were purchased from President Titanium (MA, USA) and were cut via water jet cutter to create circle substrates with a diameter of 2.54 cm and 1.22 cm for adhesive bond strength test and other characterizations, respectively. Then substrates were sandblasted and washed in deionized water and acetone alternately under ultrasonic. An optimization study was performed with 1, 3, and 5 wt.% commercial grade HA powder (Berkeley Advanced Biomaterials, Inc, Berkeley, CA) mixed with Ti6Al4V powder (ATI Powder Metals, Pittsburgh, PA) for depositing a gradient HA layer on Ti6Al4V substrates using LENS™. 3 wt.% HA was chosen as the optimum addition as 5 wt.% HA produced large cracks. LENS™ 750 (Optomec, Albuquerque, NM, USA) unit with 0.5 kW continuous wave Nd:YAG laser was used in this study. The chamber atmosphere was controlled by argon with an oxygen level less than 50 ppm to reduce the oxidation of Ti6Al4V. A single layer coating with a thickness of 0.3 mm was deposited on Ti6Al4V. The laser power, scan speed, and powder feed rate used in this study were listed in Table 1. These parameters were selected according to prior optimizations.

2.2 Plasma Sprayed HA Coating

HA powder with a particle size between 150 and 212 μm (Monsanto, USA) was used for plasma sprayed HA coating. MgO-Ag_2O-HA powder was prepared by mixing 1 wt.% MgO and 2 wt.% Ag_2O with HA using 1:1 milling media to powder ratio at 70 rpm for 2 h. Concentration of dopants was chosen based on previous optimizations in our group [24,25].

Author Manuscript Author Manuscript Author Manuscript Author Manuscript

The induction coupled RF plasma spray system (Tekna Plasma Systems, Canada) with a supersonic nozzle and axial powder feeding was used to deposit HA coatings. Four different types of samples were made including HA/Ti6Al4V, HA/LENS/Ti6Al4V, MgO-Ag_2O-HA/LENS/Ti6Al4V, and MgO Ag_2O-HA/Ti6Al4V. Table 1 also lists the plasma operating parameters used in this study. Two coating strategies and all coating compositions are presented in Fig. 1.

2.3 Phase and Chemical Group Identification, and Microstructure

An X-ray diffractometer (Siemens D5000, Aubrey, TX) using CuK_α radiation at 40 kV and 30 mA was used to identify phase formation of HA/Ti6Al4V, HA/LENS/Ti6Al4V, and MgO-Ag2O-HA/LENS/Ti6Al4V.

HA/Ti6Al4V, HA/LENS/Ti6Al4V, and MgO-Ag_2O-HA/LENS/Ti6Al4V were also scanned using Fourier Transformed Infrared Spectroscopy (FTIR) to identify their chemical groups. Coatings were faced on an ATR diamond crystal followed by scanning in the range from 400 to 1200 cm^{-1}. The final graph was achieved by plotting transmittance against wave number.

Samples for the observation of interface microstructure were mounted with polymer resin. Then cut by a low-speed diamond saw at 300 rpm to expose the interfaces. Interfaces were polished and etched followed by observation under a Field Emission Scanning Electron Microscope (FESEM).

2.4 Adhesive Bond Strength Test, Microhardness Measurements, and Surface Roughness

The adhesive bond strength was tested on HA/Ti6Al4V, HA/LENS/Ti6Al4V, and MgOAg_2O-HA/LENS/Ti6Al4V. All test parameters were based on ASTM C633. Samples were glued to two sandblasted counter posts using protocol recommended glue, Armstrong A-12 (Resin Technology Group, LLC, Easton, MA). Then glue was cured at 93°C (200 °F) for 30 min followed by the test using a standard tensile test setup at a constant crosshead speed of 0.0013 cm/s until failure. The adhesive bond strength was calculated as maximum force divided by sample area. The data is reported as mean ± standard deviation (n=3).

Microhardness was measured using a Phase II Plus, Micro Vickers hardness tester (Upper Saddle River, NJ, USA) on triplet cross-sections of HA/LENS/Ti6Al4V and MgO-Ag_2O-HA/LENS/Ti6Al4V mounted in phenolic thermoset resin and ground with grinding paper then polished. A load of 200 g and 15 s dwell time was used on the Ti6Al4V, LENS™ processed 3 wt.% HA, and plasma sprayed coating regions. A depiction of the measurements taken on each sample is shown in Fig. 2. Spacing in all directions from each measurement to the next is at least 5x the indent size as to not influence any data.

Surface roughness of Ti6Al4V, MgO-Ag_2O-HA/Ti6Al4V, and MgO-Ag_2OHA/LENS/Ti6Al4V samples were investigated in triplicate using a profilometer (SPN Technologies Inc.) with an elapsed time of 33.3 s across 5 mm at a velocity of 0.10 mm/s.

Author Manuscript Author Manuscript Author Manuscript Author Manuscript

2.5 Ag^+ release

To mimic the pH of the physiological environment, phosphate buffer solution (PBS, pH=7.4) was used as a buffer for one release study. To mimic the acidic microenvironment post injury or implantation, acetic buffer solution (pH=5) was used for a second release study. $MgOAg_2O$-HA/LENS/Ti6Al4V and MgO-Ag_2O-HA//Ti6Al4V coated samples (n=3) were immersed in 5 ml of either buffer solution at 37 °C under 150 rpm constant shaking for 17 days. Release buffer was removed and supplemented with 2 vol.% HCl and 5 vol.% HNO_3 to prevent any precipitation of ions during storage. Fresh buffer solution was replaced for each timepoint and readings were taken at a dilution factor of 6x. ICP-MS (Agilent 7700, Agilent Technologies, Inc. CA, USA) was used to measure the Ag^+ release at each time point. The temperature of the spray chamber was maintained at 2 °C. Argon gas flow conditions were 15 L/min plasma gas, 1 L/min auxiliary gas, 0.8 L/min nebulization gas, and 0.3 L/min make-up gas. Similar protocols have been followed by other researchers [26–28].

2.6 Antibacterial Disk Diffusion Test

Bacterial cultures of *Escherichia coli (E. coli)* (Carolina Biological Supply Company, Burlington, NC, USA) and *Staphylococcus aureus (S. aureus)* (Carolina Biological Supply Company, Burlington, NC, USA) in the form of MicroKwik Culture® pathogen vials were employed for the disk diffusion test. Nutrient agar was used for the *E. coli* inoculation and brain heart infusion agar was used for the *S. aureus* inoculation. Culture vials were rehydrated with respective media and left to incubate for 48 h at 37 °C. Bacterial inoculation onto the appropriate agar dishes was performed using sterile swabs and MgO-Ag2O-HA/Ti6Al4V and pure HA disc samples were placed. After 24 h of incubation at 37 °C, plates were imaged to assess the respective zones of inhibition. All procedures were followed per manufacturer recommendations. Sample compositions were tested in duplicate to ensure consistent zones of inhibition.

2.7 Osteoblast cell - materials interactions

Samples were sterilized in an autoclave at 121 °C for 20 min. Primary human osteoblasts (PromoCell, Heidelberg, Germany) was cultured for *in vitro* characterizations of coated samples. After cells reached their confluency, they were transferred onto each sample at a density of 1×10^4 cells/sample. The cell medium for this cell line was prepared by mixing osteoblast growth medium (PromoCell, Heidelberg, Germany) and osteoblast growth medium supplement mix (PromoCell, Heidelberg, Germany). Cells were incubated at 37 °C and 5 vol. % CO_2 according to the manufacturer recommended protocol for this particular cell line. Cell medium was changed every alternate day for the following 11 days.

Samples for cell morphological observation were transferred to new well plates after 3, 7, and 11 days of incubation. The samples were fixed in a 2 % paraformaldehyde/2 % glutaraldehyde in 0.1 M phosphate buffer solution overnight at 4 °C followed by a post-fixation in 2 % osmium tetroxide (OsO_4) at 4 °C overnight. After fixation, each sample was dehydrated in an ethanol series from 30 % to 100 % followed by hexamethyldisilane (HMDS) drying before gold coating. Gold coating was conducted using a Technics Hummer V sputter coater at 10 milliamps for 6 min. After gold coating, cellular morphology was observed under FESEM.

Author Manuscript Author Manuscript Author Manuscript Author Manuscript

Osteoblast proliferation was evaluated by using a 3-(4, 5-dimethylthiazol-2-yl)-2, 5-diphenyl tetrazolium bromide (MTT) assay (Sigma, St. Louis, MO). MTT assay solution was made by dissolving 50 mg MTT powder in 10 ml filter sterilized PBS. 100 μl of as prepared MTT solution and 900 μl of cell media were mixed and added to each sample followed by incubation at 37 °C for 2 h. After aspirating MTT solution, 600 μl of solubilization solution (10 % Triton X-100, 0.1 N HCl and isopropanol) was added to samples. The resulting supernatant was transferred into a 96-well plate and read by an ultraviolet-visible spectroscopy (UVS, Synergy 2 microplate reader, Biotek, Winooski, VT) at 570 nm. Three biological and technical replicates were used in MTT measurements.

Osteoblast differentiation was evaluated by an alkaline phosphatase (ALP) kit purchased from SensoLyte (Fremont, CA). The procedures used for ALP measurements were provided in the instruction recommended by the manufacturer. Briefly, cell media was first aspirated from samples. Then cells on samples were detached from the sample surface and homogenized in assay buffer followed by adding 5 mM p-nitrophenyl phosphate solution to initiate the reaction. The reaction was continued for 60 min at room temperature in a dark place. After adding the stop solution, ALP intensity was measured by using UV-Vis at 405 nm.

2.8 Statistical Analysis

Coating bond strength, hardness, ion release, MTT, and ALP tests were conducted in triplicate. Data is reported as mean ± standard deviation with statistical analysis performed with a p value < 0.05 considered significant and indicated by *.

3. Results

3.1 Phase and Chemical Group Identification and Microstructure

XRD and FTIR plots of LENS™ processed 3 wt.% HA, HA/LENS/Ti6Al4V, and Mg_2OAg O-HA/LENS/Ti6Al4V are shown in Fig. 3. LENS™ processed 3 wt.% HA shows prominent α-Ti (JCPDS# 51–0631) and β-Ti (JCPDS# 44–1288) peaks as well as small HA peaks (JCPDS# 09–0432) from the XRD plot. The FTIR plot supports the XRD result by showing small P-O symmetric stretching mode (ν_1), antisymmetric P-O stretching modes (ν_3), and antisymmetric P-O bending modes (ν_4) from HA. Both HA/LENS/Ti6Al4V and MgO-Ag_2O-HA/LENS/Ti6Al4V show major HA formation (JCPDS# 09–0432), while MgO-Ag_2O-HA/LENS/Ti6Al4V also presents a silver peak (JCPDS# 41–1402) by its XRD plot. Strong P-O symmetric stretching mode (ν_1), antisymmetric P-O stretching modes (ν_3), and antisymmetric P-O bending modes (ν_4) are observed from HA/LENS/Ti6Al4V and MgO-Ag_2O-HA/LENS/Ti6Al4V indicating their prominent HA formation.

Interface microstructures between LENS™ processed 3 wt.% HA and Ti6Al4V, HA and LENS™ processed 3 wt.% HA, and Ag O-MgO-HA and LENS™ 2 processed 3 wt.% HA are shown in Fig. 4. The interface between LENS™ processed 3 wt.% HA and Ti6Al4V can be clearly recognized in Fig. 4 (a) and (b). The thickness of the LENS™ layer is 120 μm. HA particles are distributed in the LENS™ processed 3 wt.% HA layer. For plasma sprayed HA and Ag_2O-MgO-HA coatings, they are strongly bonded with LENS™ processed 3 wt.%

Author Manuscript Author Manuscript Author Manuscript Author Manuscript

HA without any gaps. The plasma layer thickness ranges between 60 and 80 μm with an average thickness of 70 μm.

3.2 Adhesive Bond Strength, Microhardness Profile, and Surface Roughness

Adhesive bond strength for HA/Ti6Al4V, HA/LENS/Ti6Al4V, and MgO-Ag_2OHA/LENS/Ti6Al4V are shown in Fig. 5. All coatings have higher adhesive bond strength than the minimum required 15 MPa [16,29]. The presence of LENS™ processed gradient HA layer significantly increases the adhesive bond strength of plasma sprayed coatings. The presence of Ag_2O and MgO does not have significant effects on the adhesive strength of plasma sprayed HA coating. The microhardness profiles of HA/LENS/Ti6Al4V and MgO-Ag_2O-HA/LENS/Ti6Al4V are shown in Fig. 6. The profile of both coatings can be separated into three distinct regions: Ti6Al4V substrate, LENS™ processed gradient HA layer, and plasma sprayed coatings. In both coatings, the microhardness increases in the LENS™ processed gradient HA layer region compared to Ti6Al4V substrate and then significantly drops in plasma sprayed coatings region. The maximum microhardness for HA/LENS/Ti6Al4V and MgO-Ag_2O-HA/LENS/Ti6Al4V is found to be 737 ± 38 Hv and 684 ± 38 Hv, respectively, while the microhardness of Ti6Al4V is only around 398 ± 23 Hv. Surface roughness average height (Ra) of the Ti6Al4V (sandblasted), MgO-Ag2O-HA/Ti6Al4V, and MgO-Ag2O-HA/LENS/Ti6Al4V samples were 4 ± 1 μm, 14 ± 2 μm, and 16 ± 2 μm.

3.3 Ag^+ release

The accumulative Ag^+ release in PBS for MgO-Ag_2O-HA/LENS/Ti6Al4V and MgOAg2O-HA/Ti6Al4V shows a burst release in the first 3 days and reached nearly steady state onwards, as shown in Fig. 7. In acetic buffer solution, the accumulative Ag^+ release for both compositions had an initial burst release but did not quite reach a steady state release. For both dissolution plots, the accumulative Ag^+ release is notably lower than the toxic limit for the average human body with a much higher release in acetic buffer solution. In both buffer solutions, MgO-Ag_2O-HA/LENS/Ti6Al4V releases significantly less Ag^+ ions compared to without LENS.

3.4 Antibacterial Disk Diffusion Test

Antibacterial properties were observed for MgO-Ag_2O-HA/Ti6Al4V samples against *E. coli* and *S. aureus* strands of bacteria. Pure HA discs were also tested to serve as a control and showed no zone of inhibition. Doped plasma samples clearly showed zones of inhibition against both bacteria strands with a higher efficacy against *E. coli*, as shown in Fig. 8.

3.5 Cell-materials Interaction

Stretched osteoblast morphology is observed for Ti6Al4V control, HA/LENS/Ti6Al4V, and MgO-Ag_2O-HA/LENS/Ti6Al4V from day 3 to day 11, as shown in Fig. 9, however, the number of osteoblasts cannot be quantitively compared between different compositions by SEM images since the reprecipitation of coatings covers most of the cell surface. MgO-Ag_2O-HA/LENS/Ti6Al4V shows lower cell viability compared to pure HA coating at day 3 and 7, but its cell viability significantly increases at day 11 compared to day 7, which is close to the cell viability of pure HA coating, as shown in Fig. 10. In addition, coated

Author Manuscript Author Manuscript Author Manuscript Author Manuscript

samples show significantly higher cell viability compared to Ti6Al4V control at days 3, 7, and 11. All samples show low osteoblast differentiation at day 3 and 7. Osteoblast differentiation starts to increase at day 11. HA/LENS/Ti6Al4V and MgO-Ag_2O-HA/LENS/Ti6Al4V show comparable osteoblast differentiation at day 11, which is significantly higher compared to Ti6Al4V control, as shown in Fig. 11.

4. Discussion

HA coatings on titanium implants are a widely used and researched composite system for enhanced osseointegration. HA coatings provide osteoconductive properties that bare titanium implants cannot produce alone. Despite the improvements made by introducing a ceramic coating, differing thermal properties and high residual stress between coating and implant materials compromise the optimum mechanical properties [30]. Thermal stresses can be introduced during plasma spray coatings due to the rapid cooling rates. These quenching stresses can induce strain mismatches, which could lead to cracking of the plasma coatings [31,32]. In this study, LENS™ is used to create a 3 wt.% HA gradient layer incorporating a thermal barrier between Ti6Al4V and a doped HA plasma coating. This thermal barrier reduces the heat loss seen with plasma spray deposition. The thermal conductivity of Ti6Al4V is 19 W m^{-1} K^{-1} [33] and HA is 0.7–2.2 W m^{-1} K^{-1} [34]. Thermal diffusivity of Ti6Al4V is 2.2×10^{-6} m^2 s^{-1} [33] and plasma sprayed HA is $0.29 \pm 0.05 \times 10^{-6}$ m^2 s^{-1} [35]. With the addition of 3 wt.% HA into the Ti6Al4V powder preparation for the LENS™ layer, the thermal diffusivity from Ti6Al4V would decrease therefore creating a thermal barrier between the Ti6Al4V samples with the plasma HA coating. In doing so, the crystallinity of the plasma coating is retained or even enhanced. The silver ion release in this study supports the hypothesis that the gradient layer enhanced crystallinity by reducing the release compared to control.

Silver has been employed as an antimicrobial agent for centuries and can be seen in many medical devices such as catheters and even everyday items like door handles [36–38]. The use of silver in this system can offer remarkable antimicrobial effects for orthopedic implants to prevent secondary infections [39–41]. The use of silver as a coating in biomedical devices has been approved by the US Food and Drug Administration (FDA). The use of dopants in this study is not only beneficial to the overall system for osseointegration and infection control but can be useful in analyzing crystallinity of the surface modifications. In this study, two pHs were used to evaluate the release kinetics of the doped MgO and Ag_2O plasma coating with the LENS™ gradient layer and without. One reason to test the coating durability in an acidic environment (pH=5) is to mimic orthopedic surgery practices. During orthopedic surgery, tranexamic acid is commonly used for bleeding control leading to an acidic environment near the surgery site [42,43]. The burst Ag^+ release should not exceed 10 ppm to stay within toxic levels which was the case in this study [44]. Post-surgery, the implant will stay in the physiological environment (pH=7). Our study utilizes PBS (pH=7.4) to ensure long-term Ag^+ release below the toxic limit for healthy integration between implant and host tissue as well as provide effective secondary infection control. In both buffer solutions, the LENS™ gradient layer produced significantly less release compared to without. In PBS, the LENS™ gradient layer released 70 % less and in acetic buffer, the LENS™ gradient layer released 73 % less compared to without. With more

Author Manuscript Author Manuscript Author Manuscript Author Manuscript

amorphous phase in the just doped HA plasma coating, the dissolution rate increased due to the randomized, short-range order of the lattice. With the LENS™ gradient layer, the release significantly decreased indicating higher crystallinity of the plasma coating. The lattice of a crystalline solid is held together uniformly via the intermolecular forces. Crystalline phase enhances the ability of the coating to withstand the constant shaking in the buffer solutions compared to a more amorphous coating. This phenomenon of an increased level of crystallinity decreasing the dissolution rate and reducing the amount of ions released has been explored by other researchers as well [45]. For pharmaceutics, researchers will actually try to enhance dissolution properties to enable better saturated drugs within the body through increasing amorphous phase of their system [46–48].

The presence of a LENS™ processed gradient HA layer not only enhanced crystallinity but also significantly increased the adhesive bond strength of plasma sprayed HA coating by 52 %. Bond strength is determined by the weakest bonding interface and in this case, would be the interface between HA plasma coating and the LENS™ layer. Several studies have reported calcium phosphate coating on titanium based substrates by laser deposition with one above 50 MPa adhesive bond strength [49,50]. HA plasma coatings on titanium show much less adhesive bond strength on their own, as seen in this work and others [24,51,52]. LENS™ processing can create a pattern on the substrate thereby increasing the surface area as seen in Fig. 1 and enhancing the coating adherence by plasma spray deposition. The gradient HA LENS™ layer also decreases the challenges faced by the mismatch in coefficients of thermal expansion that inhibit the coating bond strength. The thermal expansion coefficient of titanium is $9–10 \times 10^{-6}$ / °C and HA is 12×10^{-6} / °C [53]. By utilizing a composition of 3 wt.% HA into Ti6Al4V powder during LENS™ layer processing, the thermal expansion coefficient of the gradient HA layer will be between the coefficients of Ti and HA.

In creating the LENS™ layer, a small wt.% of HA must be incorporated to avoid high mismatches in thermal expansion coefficients between the gradient layer and Ti6Al4V substrate. If too much HA is added into the gradient layer, the mismatch becomes a critical issue just as the mismatch between just a plasma coating and Ti6Al4V substrate. A notable mismatch could lead to residual stresses that cause cracking. A singular pass of the LENS™ was employed to lessen the amount of heat exposure that could cause residual stresses. These parameters enabled a crack-free Ti6Al4V-HA interlayer by LENS™ processing, as shown in Fig. 4 (a). HA is evenly distributed within the Ti6Al4V matrix and a clear interface between deposited and substrate material is observed in Fig. 4 (b). In this study, no phase transformation of the HA is seen which is an improvement to our last study [15]. HA and titanium were the only phases present in the Ti6Al4V-HA interlayer as shown in Fig. 3. A phase transformation is not beneficial to the osteoconductivity and the overall lifespan of coated implants. The processing parameter differs from the previous study by using a laser power of 400 W instead of 500 W as well as a shorter laser reaction time thereby preventing undesired phase transformations.

Evaluation of the doped coating *in vitro* with an osteoblast cell line shows significantly enhanced proliferation and differentiation with the presence of any HA coating. It should be noted that despite reprecipitation of the HA coating causing difficulties to see cellular

Author Manuscript Author Manuscript Author Manuscript Author Manuscript

morphology by SEM images due to covering the cells, surface roughness plays a key role in cellular attachment. Researchers have found higher cellular attachment to surfaces when surfaces were rough compared to smooth counterparts [54–56]. The surface roughness did not significantly change between plasma coated samples with or without LENS however both provided significantly rougher surfaces compared to Ti6Al4V samples. MgO was reported to increase osteoconductivity by improving the osteoblast attachment, proliferation, and alkaline phosphatase production *in vitro* [25]. An *in vivo* study utilizing rabbit femoral defects also showed the presence of MgO in HA enhanced osteogenesis [57]. In this study, the combination of MgO and Ag_2O had no deleterious effects on proliferation and differentiation of osteoblast cells compared to pure HA coating as control. The doped HA coating also showed zones of inhibition against bacterial strands of *E. coli* and *S. aureus,* a gram-negative and a gram-positive bacteria, respectively. Incubation time was limited to 24 h to ensure reliable data between each sample testing. Beyond this incubation time, results can become highly unreliable [58]. This indicates the dopants do not negatively affect the benefits of HA coatings and can provide infection control that would otherwise be absent.

5. Conclusions

A gradient HA coating was processed using a 3 wt.% HA layer by LENS™ followed by plasma sprayed MgO-Ag_2O-HA coating on Ti6Al4V substrates. Both interfaces were strongly bonded without any gaps. The adhesive bond strength increased by 52% with the gradient HA LENS™ compared to without due to the thermal barrier the LENS™ layer creates. This barrier reduces fast quenching and diminishes the prominent difference in coefficient of thermal expansion between the plasma coating and substrate. The presence of MgO and Ag_2O had no significant effects on the adhesive bond strength of the coating nor negative effects on osteoblast proliferation or differentiation by day 11 but provided a long-term silver release below the toxic limit for preventing non-aseptic loosening of implants. This novel gradient surface modification system can improve osseointegration for patients with active lifestyles and decrease the risk of load-bearing implant failure from loosening or infection.

Acknowledgements

The authors would like to thank Dr. Himanshu Sahasrabudhe for his help with fabricating LENS processed samples. Authors would also like to acknowledge financial support from the National Institute of Arthritis and Musculoskeletal and Skin Diseases of the National Institutes of Health under award number 1R01AR066361. The content is solely the responsibility of the authors and does not necessarily represent the official views of the National Institutes of Health.

References

[1]. Wolford M, Paso K, Bercovitz A, Hospitalization of Total Hip Replacement Among Inpatients Aged 45 and Over: United States, NCHS Data Brief, 2010.2015 (2000) 186.

[2]. Sargeant A, Goswami T, Hip Implants: Paper V. Physiological Effects, Materials & Design, 27 (2006) 287–307.

[3]. Mudge RP, Wald NR, Laser Engineered Net Shaping Advances Additive Manufacturing and Repair, Welding Journal-New York-, 86 (2007) 44.

Author Manuscript Author Manuscript Author Manuscript Author Manuscript

[4]. Ning F, Hu Y, Liu Z, wang X, Li Y, Cong W, Ultrasonic Vibration-Assisted Laser Engineered Net Shaping of Inconel 718 Parts: Microstructural and Mechanical Characterization, Journal of Manufacturing Science and Engineering, 140 (2018) 061012.

[5]. Kunce I, Polanski M, Karczewski K, Plocinski T, Kurzydlowski KJ, Microstructural Characterisation of High-Entropy Alloy AlCoCrFeNi Fabricated by Laser Engineered Net Shaping, Journal of Alloys and Compounds, 648 (2015) 751–758.

[6]. Li Y, Hu Y, Cong W, Zhi L, Guo Z, Additive Manufacturing of Alumina Using Laser Engineered Net Shaping: Effects of Deposition Variables, Ceramics International, 43 (2017) 7768–7775.

[7]. Bose S, Ke D, Sahasrabudhe H, Bandyopadhyay A, Additive Manufacturing of Biomaterials, Prog. Mater. Sci 93 (2018) 45–111.

[8]. Attar H, Ehtemam-Haghighi S, Kent D, Wu X, Dargusch MS, Comparative Study of Commercially Pure Titanium Produced by Laser Engineered Net Shaping, Selective Laser Melting and Casting Processes, Materials Science and Engineering: A, 705 (2017) 385–393.

[9]. Balla VK, Banerjee S, Bose S, Bandyopadhyay A, Direct Laser Processing of a Tantalum Coating on Titanium for Bone Replacement Structures, Acta Biomater. 6 (2010) 2329–2334. [PubMed: 19931654]

[10]. Roy M, Balla VK, Bandyopadhyay A, Bose S, MgO-doped Tantalum Coating on Ti: Microstructural Study and Biocompatibility Evaluation, ACS Applied Materials & Interfaces, 4 (2012) 577–580. [PubMed: 22248182]

[11]. Han C, Li Y, Wang Q, Cai D, Wei Q, Yang L, Wen S, Liu J, Shi Y, Titanium/Hydroxyapatite (Ti/HA) Gradient Materials with Quasi-Continuous Ratios Fabricated by SLM: Material Interface and Fracture Toughness, Materials & Design, 141 (2018)256–266.

[12]. Han C, Wang Q, Song B, Li W, Wei Q, Wen S, Liu J, Shi Y, Microstructure and Property Evolutions of Titanium/Nano-Hydroxyapatite Composites in-situ Prepared by Selective Laser Melting, J. Mech. Behav. Biomed. Mater 71 (2017) 85–94. [PubMed: 28267662]

[13]. Morais LS, Serra GG, Muller CA, Andrade LR, Palermo EFA, Elias CN, Meyers M, Titanium Alloy Mini-implants for Orthodontic Anchorage: Immediate Loading and Metal Ion Release, Acta Biomater. 3 (2007) 331–339. [PubMed: 17257912]

[14]. Wölfle JV, Fiedler J, Dürselen L, Reichert J, Scharnweber D, Förster A, Schwenzer B, Reichel H, Ignatius A, Brenner RE, Improved Anchorage of Ti6Al4V Orthopaedic Bone Implants through Oligonucleotide Mediated Immobilization of BMP-2 in Osteoporotic Rats, PLOS ONE, 9 (2014) e86151. [PubMed: 24465929]

[15]. Roy M, Balla VK, Bandyopadhyay A, Bose S, Compositionally Graded Hydroxyapatite/ Tricalcium Phosphate Coating on Ti by Laser and Induction Plasma, Acta Biomater. 7 (2011) 866–873. [PubMed: 20854939]

[16]. Roy M, Bandyopadhyay A, Bose S, Induction Plasma Sprayed Nano Hydroxyapatite Coatings on Titanium for Orthopaedic and Dental Implants, Surf. Coat. Technol 205 (2011)2785–2792. [PubMed: 21552358]

[17]. Rau JV, Cacciotti I, Laureti S, Fosca M, Varvaro G, Latini A, Bioactive, Nanostructured Si-Substituted Hydroxyapatite Coatings on Titanium Prepared by Pulsed Laser Deposition, Journal of Biomedical Materials Research Part B: Applied Biomaterials, 103 (2015) 1621–1631.

[18]. Zhong Z, Qin J, Ma J, Electrophoretic Deposition of Biomimetic Zinc Substituted Hydroxyapatite Coatings with Chitosan and Carbon Nanotubes on Titanium, Ceramics International, 41 (2015) 8878–8884.

[19]. Aruna ST, Kulkarni S, Chakraborty M, Senthil Kumar S, Balaji N, Mandal C, A Comparative Study on the Synthesis and Properties of Suspension and Solution Precursor Plasma Sprayed Hydroxyapatite Coatings, Ceramics International, 43 (2017) 9715–9722.

[20]. Ke D, Robertson SF, Dernell WS, Bandyopadhyay A, Bose S, Effects of MgO and SiO2 on Plasma-Sprayed Hydroxyapatite Coating: An in Vivo Study in Rat Distal Femoral Defects, ACS Applied Materials & Interfaces, 9 (2017) 25731–25737. [PubMed: 28752993]

[21]. Mejias A, Candidato RT Jr., L. Pawlowski, D. Chicot, Mechanical Properties by Instrumented Indentation of Solution Precursor Plasma Sprayed Hydroxyapatite Coatings: Analysis of Microstructural Effect, Surface and Coatings Technology, 298 (2016)93–102.

Author Manuscript Author Manuscript Author Manuscript Author Manuscript

[22]. Hasan MF, Wang J, Berndt C, Evaluation of the Mechanical Properties of Plasma Sprayed Hydroxyapatite Coatings, Applied Surface Science, 303 (2014) 155–162.

[23]. Maier JAM, Bernardini D, Rayssiguier Y, Mazur A, High Concentrations of Magnesium Modulate Vascular Endothelial Cell Behaviour in vitro, Biochim. Biophys. Acta 1689 (2004) 6–12. [PubMed: 15158908]

[24]. Fielding G, Roy M, Bandyopadhyay A, Bose S, Antibacterial and Biological Characteristics of Plasma Sprayed Silver and Strontium Doped Hydroxyapatite Coatings, Acta Biomater. 8 (2012) 3144–3152. [PubMed: 22487928]

[25]. Xue W, Dahlquist K, Banerjee A, Bandyopadhyay A, Bose S, Synthesis and Characterization of Tricalcium Phosphate with Zn and Mg Based Dopants, J. Mater. Sci. Mater. Med 19 (2008) 2669–2677. [PubMed: 18270806]

[26]. Hoover S, Tarafder S, Bandyopadhyay A, Bose S, Silver doped resorbable tricalcium phosphate scaffolds for bone graft applications, Materials Science and Engineering: C, 79 (2017) 763–769.

[27]. Zhao L, Wang H, Huo K, Cui L, Zhang W, Ni H, Zhang Y, Wu Z, Chu PK, Antibacterial nano-structured titania coating incorporated with silver nanoparticles, Biomaterials, 32 (2011) 5706–5716. [PubMed: 21565401]

[28]. Chen Y, Zheng X, Xie Y, Ji H, Ding C, Li H, Dai K, Silver release from silver-containing hydroxyapatite coatings, Surface and coatings technology, 205 (2010) 1892–1896.

[29]. Søballe K, Hydroxyapatite Ceramic Coating for Bone Implant Fixation. Mechanical and Histological Studies in Dogs, Acta Orthop. Scand. Suppl 255 (1993) 1–58. [PubMed: 8237337]

[30]. Dapei T, Thermal-Mechanical Coupling in Plasma-Sprayed Hydroxyapatite Coating on Ti-6Al-4V Substrate, Rare Met. Mater. Eng 46 (2017) 1508–1511.

[31]. Balani K, Anderson R, Laha T, Andara M, Tercero J, Crumpler E, Agarwal A, Plasma-sprayed carbon nanotube reinforced hydroxyapatite coatings and their interaction with human osteoblasts in vitro, Biomaterials, 28 (2007) 618–624. [PubMed: 17007921]

[32]. Tsui YC, Doyle C, Clyne TW, Plasma sprayed hydroxyapatite coatings on titanium substrates Part 1: Mechanical properties and residual stress levels, Biomaterials, 19 (1998) 2015–2029. [PubMed: 9870753]

[33]. Senthil Selvan J, Subramanian K, Nath AK, Kumar H, Ramachandra C, Ravindranathan SP, Laser boronising of Ti-6Al-4V as a result of laser alloying with preplaced BN, Materials Science and Engineering: A, 260 (1999) 178–187.

[34]. Clyne TW, Tsui YC, The effect of intermediate layers on residual stress distributions and debonding of sprayed thermal barrier coatings, FGM, 94 (1995) 129–136.

[35]. Bento AC, Almond DP, Brown SR, Turner IG, Thermal and optical characterization of the calcium phosphate biomaterial hydroxyapatite, Journal of Applied Physics, 79 (1996) 6848–6852.

[36]. Wang R, Neoh KG, Kang E, Tambyah PA, Chiong E, Antifouling Coating with Controllable and Sustained Silver Release for Long- Term Inhibition of Infection and Encrustation in Urinary Catheters, Journal of Biomedical Materials Research Part B: Applied Biomaterials, 103 (2015) 519–528.

[37]. Chopra I, The Increasing use of Silver-Based Products as Antimicrobial Agents: a Useful Development or a Cause for Concern? J Antimic Chem. 59 (2007) 587–590.

[38]. Monteiro DR, Gorup LF, Takamiya AS, Ruvollo-Filho AC, Camargo ER, Barbosa DB, The Growing Importance of Materials that Prevent Microbial Adhesion: Antimicrobial Effect of Medical Devices Containing Silver, Intl J Antimic Ag. 34 (2009) 103–110.

[39]. Bosetti M, Massè A, Tobin E, Cannas M, Silver Coated Materials for External Fixation Devices: in vitro Biocompatibility and Genotoxicity, Biomaterials, 23 (2002) 887–892. [PubMed: 11771707]

[40]. DeVasConCellos P, Bose S, Beyenal H, Bandyopadhyay A, Zirkle LG, Antimicrobial Particulate Silver Coatings on Stainless Steel Implants for Fracture Management, Mater. Sci. Eng. C, 32 (2012) 1112–1120.

[41]. Schierholz JM, Lucas LJ, Rump A, Pulverer G, Efficacy of Silver-Coated Medical Devices, J. Hosp. Infect 40 (1998) 257–262. [PubMed: 9868616]

Author Manuscript Author Manuscript Author Manuscript Author Manuscript

[42]. Poeran J, Rasul R, Suzuki S, Danninger T, Mazumdar M, Opperer M, Boettner F, Memtsoudis SG, Tranexamic Acid use and Postoperative Outcomes in Patients Undergoing Total Hip or Knee Arthroplasty in the United States: Retrospective Analysis of Effectiveness and Safety, BMJ, 349 (2014) g4829. [PubMed: 25116268]

[43]. Huang F, Wu D, Ma G, Yin Z, Wang Q, The use of Tranexamic Acid to Reduce Blood Loss and Transfusion in Major Orthopedic Surgery: a Meta-Analysis, J. Surg. Res 186 (2014)318–327. [PubMed: 24075404]

[44]. Greulich C, Braun D, Peetsch A, Diendorf J, Siebers B, Epple M, Köller M, The Toxic Effect of Silver Ions and Silver Nanoparticles Towards Bacteria and Human Cells Occurs in the Same Concentration Range, RSC Adv 2 (2012) 6981–6987.

[45]. Fazan F, Marquis PM, Dissolution behavior of plasma-sprayed hydroxyapatite coatings, Journal of materials science: Materials in Medicine, 11 (2000) 787–792. [PubMed: 15348061]

[46]. Alonzo DE, Zhang GGZ, Zhou D, Gao Y, Taylor LS, Understanding the behavior of amorphous pharmaceutical systems during dissolution, Pharmaceutical research, 27 (2010) 608–618. [PubMed: 20151181]

[47]. Van den Mooter G, The use of amorphous solid dispersions: A formulation strategy to overcome poor solubility and dissolution rate, Drug Discovery Today: Technologies, 9 (2012) e79–e85.

[48]. Allesø M, Chieng N, Rehder S, Rantanen J, Rades T, Aaltonen J, Enhanced dissolution rate and synchronized release of drugs in binary systems through formulation: Amorphous naproxen-cimetidine mixtures prepared by mechanical activation, Journal of Controlled Release, 136 (2009) 45–53. [PubMed: 19331842]

[49]. Roy M, Krishna BV, Bandyopadhyay A, Bose S, Laser Processing of Bioactive Tricalcium Phosphate Coating on Titanium for Load-Bearing Implants, Acta Biomater. 4 (2008)324–333. [PubMed: 18039597]

[50]. Gao Y, Hu J, Guan TH, Wu J, Zhang CB, Gao B, Physical Properties and Cellular Responses to Calcium Phosphate Coating Produced by Laser Rapid Forming on Titanium, Lasers Med. Sci 29 (2014) 9–17. [PubMed: 23139072]

[51]. Zheng X, Huang M, Ding C, Bond Strength of Plasma-Sprayed Hydroxyapatite/Ti Composite Coatings, Biomaterials, 21 (2000) 841–849. [PubMed: 10721753]

[52]. Yang Y, Chang E, Influence of Residual Stress on Bonding Strength and Fracture of Plasma-Sprayed Hydroxyapatite Coatings on Ti-6Al-4V Substrate, Biomaterials, 22 (2001) 1827–1836. [PubMed: 11396887]

[53]. Sun L, Berndt CC, Gross KA, Kucuk A, Material fundamentals and clinical performance of plasma-sprayed hydroxyapatite coatings: A review, Journal of Biomedical Materials Research: An Official Journal of The Society for Biomaterials, The Japanese Society for Biomaterials, and The Australian Society for Biomaterials and the Korean Society for Biomaterials, 58 (2001) 570–592.

[54]. Zareidoost A, Yousefpour M, Ghaseme B, Amanzadeh A, The relationship of surface roughness and cell response of chemical surface modification of titanium, Journal of Materials Science: Materials in Medicine, 23 (2012) 1479–1488. [PubMed: 22460230]

[55]. Rosales-Leal JI, Rodríguez-Valverde MA, Mazzaglia G, Ramón-Torregrosa PJ, Díaz-Rodríguez L, García-Martínez O, Vallecillo-Capilla M, Ruiz C, Cabrerizo-Vílchez MA, Effect of roughness, wettability and morphology of engineered titanium surfaces on osteoblast-like cell adhesion, Colloids and Surfaces A: Physicochemical and Engineering Aspects, 365, (2010) 222–229.

[56]. Biazar E, Heidari M, Asefnezhad A, Montazeri N, The relationship between cellular adhesion and surface roughness in polystyrene modified by microwave plasma radiation, International journal of nanomedicine, 6 (2011) 631. [PubMed: 21698084]

[57]. Landi E, Logroscino G, Proietti L, Tampieri A, Sandri M, Sprio S, Biomimetic Mg-Substituted Hydroxyapatite: From Synthesis to in vivo Behaviour, J. Mater. Sci. Mater. Med 19 (2008) 239–247. [PubMed: 17597369]

[58]. Mulligan ME, Citron DM, Kwok RY, Wheelock JP, Farrohi FK, Hindler JA, Johnston L, Impact of prolonged incubation on disk diffusion susceptibility test results for Staphylococcus aureus, Journal of clinical microbiology, 25, (1987) 840–844. [PubMed: 3584420]

Author Manuscript Author Manuscript Author Manuscript Author Manuscript

Statement of Significance

Implants are commonly composed of metals that lack osteoconductivity. Osteoconductivity is a propriety where bone grows on the surface meaning the material is compatible with the surrounding bone tissue. Plasma sprayed hydroxyapatite (HA) coating improves the osteoconductivity of metallic implants however the adhesive bond strength can be weak. This study incorporates a gradient HA coating by using an additive manufacturing technique, laser engineered net shaping (LENS™), followed by plasma spray deposition to enhance the adhesive bond strength by incorporating a thermal barrier. The proposed system has not been well studied in the current literature and the results presented bring forth an innovative way to improve the interfacial mechanical properties of plasma sprayed HA coating for load-bearing orthopedic implants.

Author Manuscript Author Manuscript Author Manuscript Author Manuscript

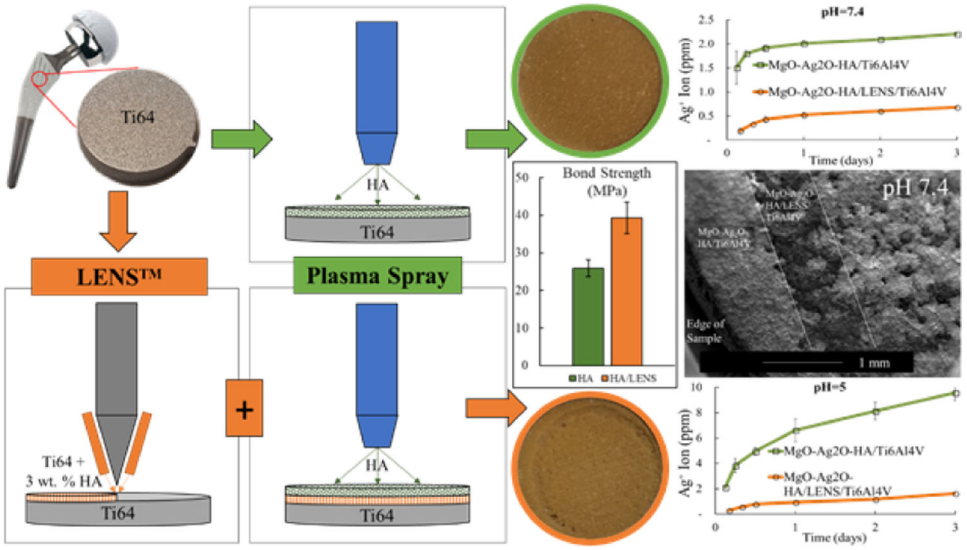

Fig. 1.

Schematic of the work showing modified surface topography with a LENS™ layer compared to without. Figures show higher coating bond strength and less ion release indicating higher crystallinity with a LENS™ layer compared to just plasma.

Author Manuscript Author Manuscript Author Manuscript Author Manuscript

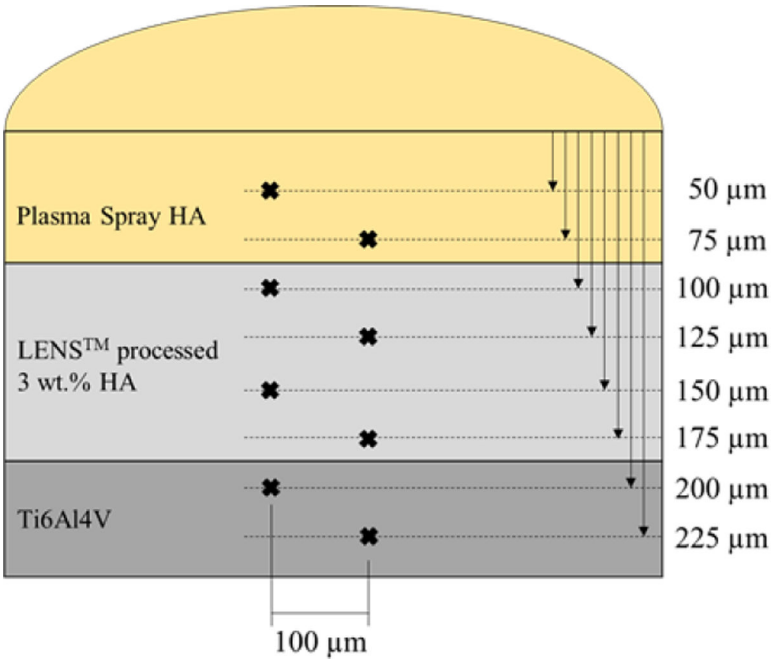

Fig. 2.

Depiction of microhardness measurements on each sample (not to scale). Indents are spaced apart radially by at least 5x the indent size.

Author Manuscript Author Manuscript Author Manuscript Author Manuscript

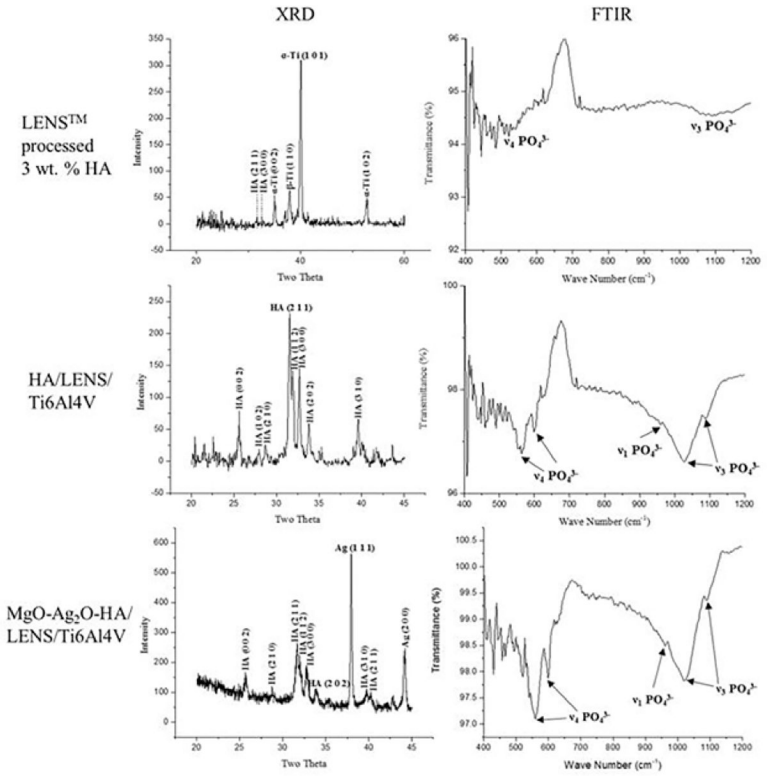

Fig. 3.

XRD and FTIR plots of LENS™ processed 3 wt.% HA, HA/LENS/Ti6Al4V, and $MgOAg_2O$-HA/LENS/Ti6Al4V showing a little amount of HA phase in LENS™ processed 3 wt.% HA, prominent HA phase in HA/LENS/Ti6Al4V, as well as HA and Ag phases in MgO-Ag_2OHA/LENS/Ti6Al4V.

Author Manuscript Author Manuscript Author Manuscript Author Manuscript

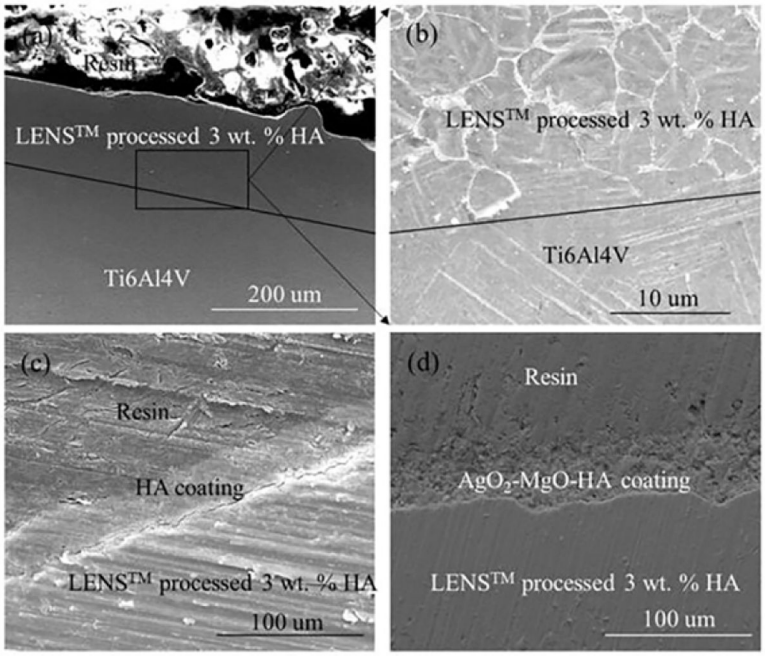

Fig. 4.

Interface microstructures between LENS™ processed 3 wt.% HA and Ti6Al4V (a)-(b), HA and LENS™ processed 3 wt.% HA (c), and Ag_2O-MgO-HA and LENS™ processed 3 wt.% HA (d) showing their strong bonding without any gaps or cracks. Lines marked in (a) and (b) are the interfaces between LENS™ processed 3 wt.% HA and Ti6Al4V. (b) is the image from the interface of (a) in high magnification. Distributed HA can be seen in (b) as white agglomerated particles.

Author Manuscript Author Manuscript Author Manuscript Author Manuscript

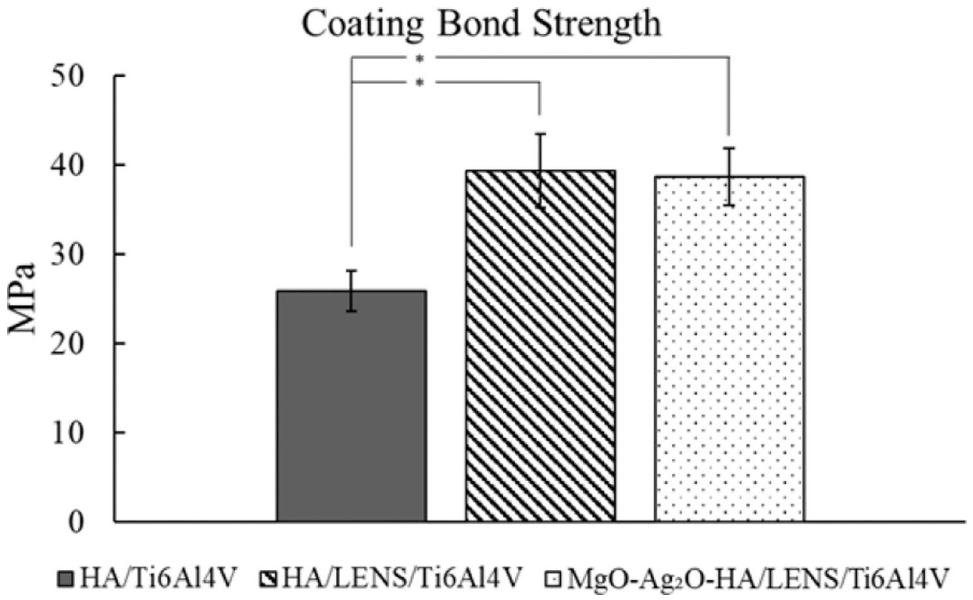

Fig. 5.

Adhesive bond strength of plasma sprayed HA and Ag_2O-MgO-HA coatings on Ti6Al4V or LENS/Ti6Al4V showing significant strength increase with LENS compared to without (* $p < 0.05$). Addition of dopants does not significantly change the plasma sprayed coating bond strength.

Author Manuscript Author Manuscript Author Manuscript Author Manuscript

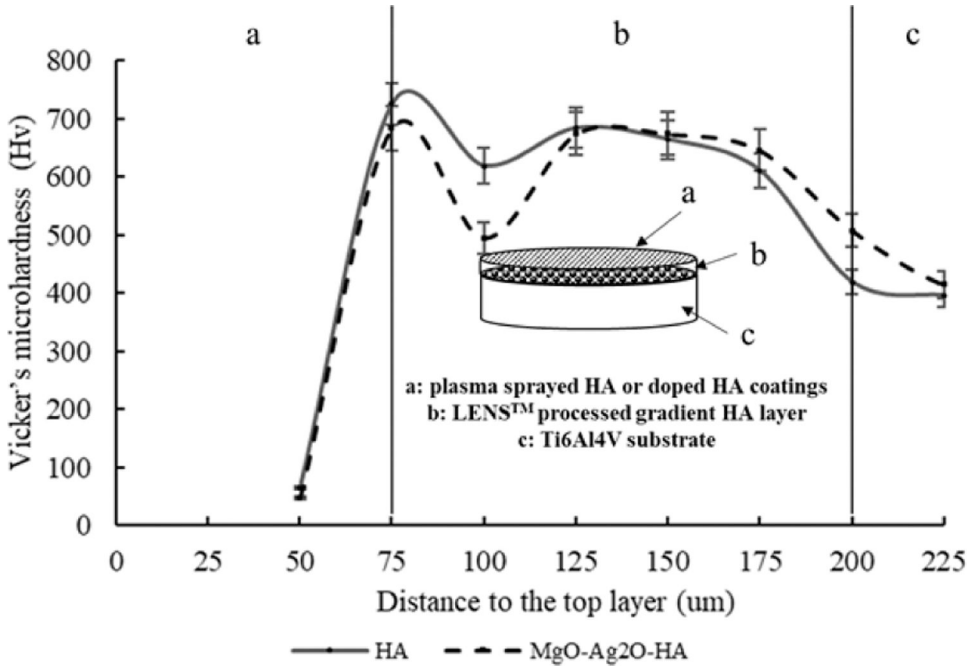

Fig. 6.

Microhardness profile of compositionally graded HA coating and HA coating doped with Ag_2O and MgO showing the microhardness improvement in the LENS™ processed gradient HA layer compared to plasma coating layer and Ti6Al4V substrate.

Author Manuscript Author Manuscript Author Manuscript Author Manuscript

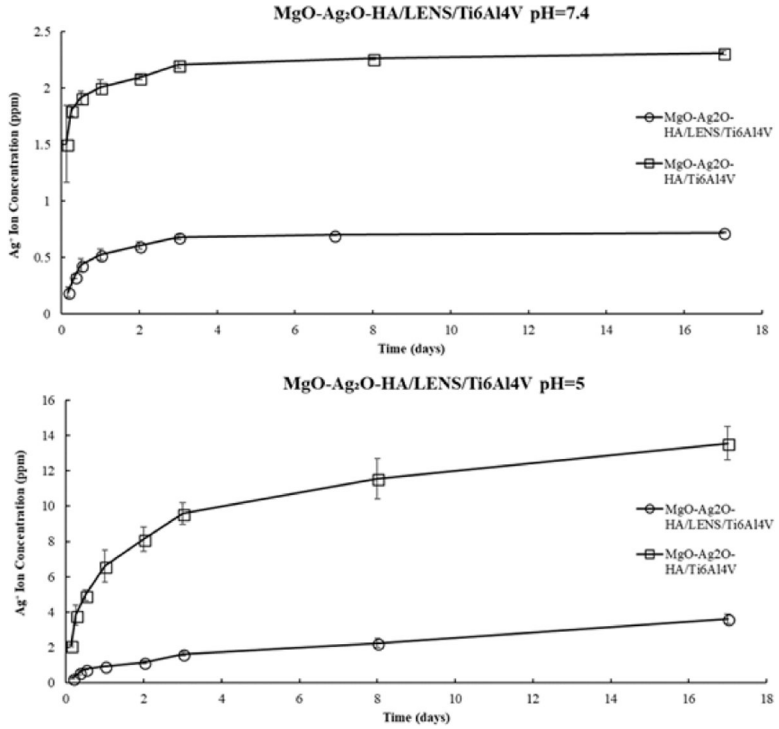

Fig. 7.

Accumulative Ag^+ release from MgO-Ag_2O-HA/LENS/Ti6Al4V and MgO-Ag_2OHA/Ti6Al4V in PBS (pH=7.4) and acetic buffer solution (pH=5) at 37 °C for 17 days showing 70% and 73% less release with a LENS layer, respectively.

Author Manuscript Author Manuscript Author Manuscript Author Manuscript

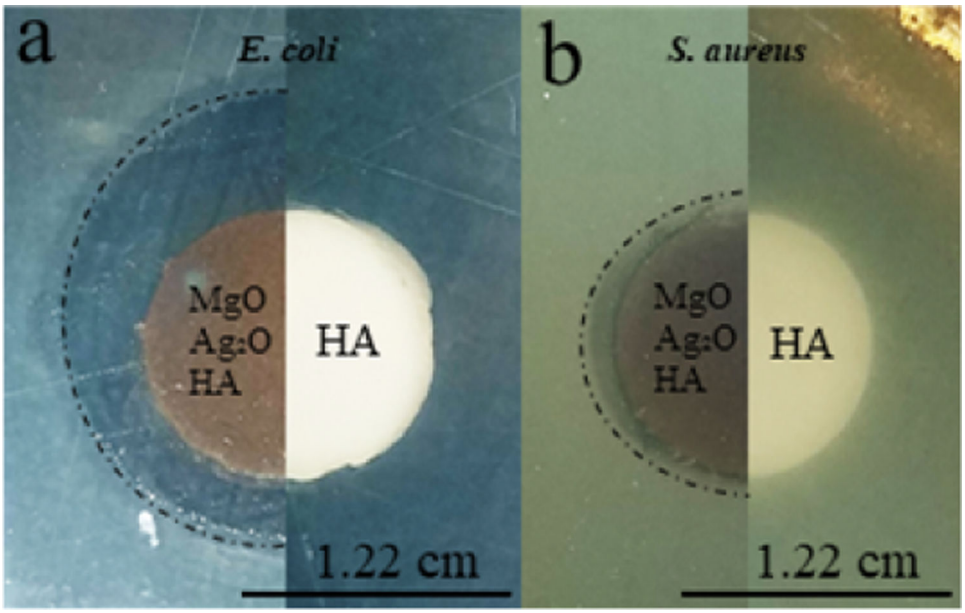

Fig. 8.

Disk diffusion test of MgO-Ag_2O-HA/Ti6Al4V and pure HA disc samples against (a) *Escherichia coli* and (b) *Staphylococcus aureus.* Clear zones of inhibition can be seen with doped plasma coated samples (left) whereas control HA samples (right) show no antibacterial properties.

Author Manuscript Author Manuscript Author Manuscript Author Manuscript

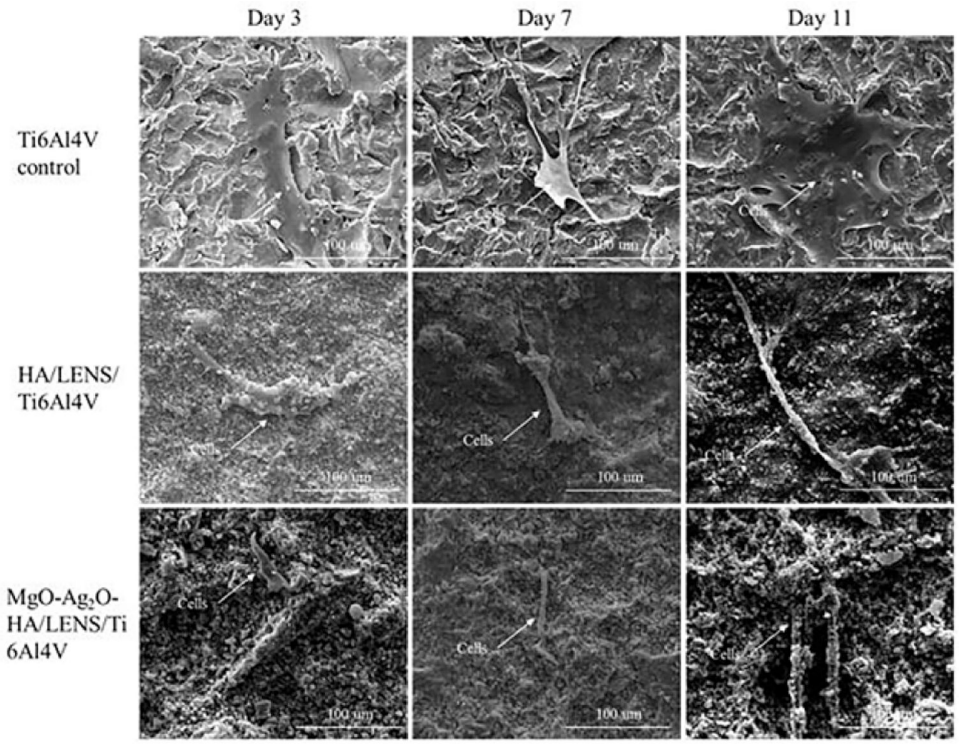

Fig. 9.

Microstructure of Ti6Al4V control, HA/LENS/Ti6Al4V, and MgO-Ag_2OHA/LENS/Ti6Al4V during the cell culture at day 3, 7, and 11 showing stretched osteoblast morphology.

Author Manuscript Author Manuscript Author Manuscript Author Manuscript

Fig. 10.

MTT assay of Ti6Al4V, HA/LENS/Ti6Al4V, and MgO-Ag_2O-HA/LENS/Ti6Al4V after 3, 7, and 11 days of cell culture showing decreased cell viability at day 3 and 7, but comparable cell viability at day 11 for MgO-Ag_2O-HA/LENS/Ti6Al4V compared to HA/LENS/Ti6Al4V (n=3. *p<0.05).

Author Manuscript Author Manuscript Author Manuscript Author Manuscript

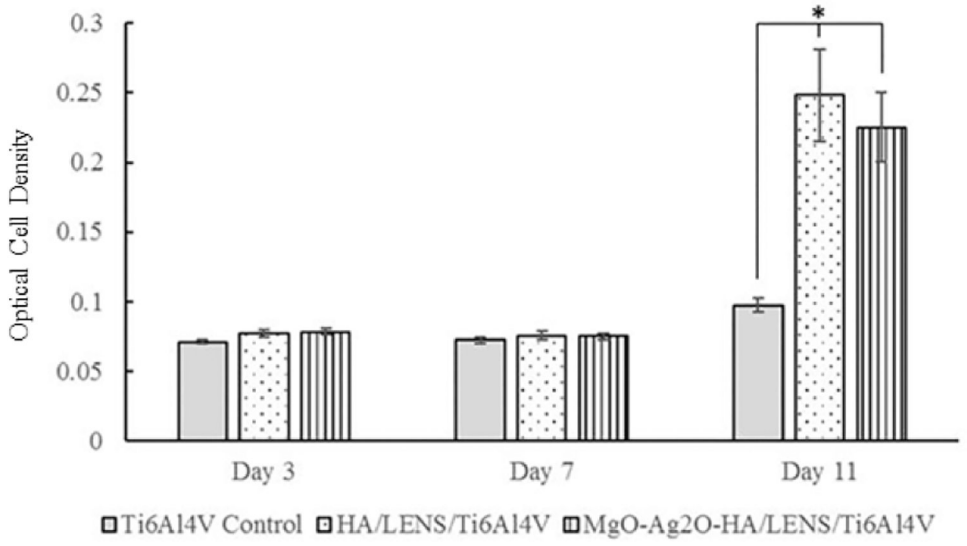

Fig. 11.

ALP assay of Ti6Al4V, HA/LENS/Ti6Al4V, and MgO-Ag_2O-HA/LENS/Ti6Al4V after 3, 7, and 11 days of cell culture showing comparable osteoblast differentiation for HA/LENS/Ti6Al4V and MgO-Ag_2O-HA/LENS/Ti6Al4V at day 11 (n=3. *$p<0.05$).

Author Manuscript

Author Manuscript

Author Manuscript

Author Manuscript

Table 1

Processing parameters of LENS™ and plasma spray deposition.

Processing parameters of LENSThl	
Laser power	400 W
Laser scan speed	17 mm 5^{-1}
Powder feed rate	15 g mind
Processing parameters of plasma spray deposition	
Central gas flow rate (s.l.p.m.)	25 Ar
Sheath gas flow rate (s.l.p.m.)	60 Ar + 6 H-)
Carrier gas flow rate (s.l.p.m.)	10 Ar
Powder (1cW)	25
Worlcing coordinate (mm)	100